ELSEVIER

Chemical Engineering Science 62 (2007) 2989–3007

Chemical Engineering Science

www.elsevier.com/locate/ces

Fluidised bed membrane reactor for ultrapure hydrogen production via methane steam reforming: Experimental demonstration and model validation

Charudatta S. Patil, Martin van Sint Annaland*, J.A.M. Kuipers

Fundamentals of Chemical Reaction Engineering, Faculty of Science and Technology, University of Twente, P.O. Box 217, 7500 AE, The Netherlands

Received 17 September 2006; received in revised form 13 February 2007; accepted 13 February 2007
Available online 24 February 2007

Abstract

Hydrogen is emerging as a future alternative for mobile and stationary energy carriers in addition to its use in chemical and petrochemical applications. A novel multifunctional reactor concept has been developed for the production of ultrapure hydrogen (< 10 ppm CO) from light hydrocarbons such as methane for online use in downstream polymer electrolyte membrane fuel cells. A high degree of process intensification can be achieved by integrating perm-selective hydrogen membranes for selective hydrogen removal to shift the methane steam reforming and water–gas-shift equilibriums in the favourable direction and perm-selective oxygen membranes for selective oxygen addition to supply the required reaction energy via partial oxidation of part of the methane feed and enable pure CO_2 capture without costly post-treatment. This can be achieved in a proposed novel multifunctional bi-membrane bi-section fluidised bed reactor [Patil, C.S., van Sint Annaland, M., Kuipers, J.A.M., 2005. Design of a novel autothermal membrane assisted fluidized bed reactor for the production of ultrapure hydrogen from methane. Industrial and Engineering Chemistry Research 44, 9502–9512]. In this paper, an experimental proof of principle for the steam reforming/water–gas-shift section of the proposed novel fluidised bed membrane reactor is presented. A fluidised bed membrane reactor for steam reforming of methane/water–gas-shift on a commercial noble metal-based catalyst has been designed and constructed using 10 H_2 perm-selective Pd membranes for a fuel cell power output in the range of 50–100 W. It has been experimentally demonstrated that by the insertion of the membranes in the fluidised bed, the thermodynamic equilibrium constraints can indeed be overcome, i.e., increased CH_4 conversion, decreased CO selectivity and higher product yield (H_2 produced/CH_4 reacted). Experiments at different superficial gas velocities and also at different temperatures and pressures (carried out in the regime without kinetic limitations) revealed enhanced reactor performance at higher temperatures (650 °C) and pressures (3–4 bar). With a phenomenological two-phase reactor model for the fluidised bed membrane reactor, incorporating a separately developed lumped flux expression for the H_2 permeation rate through the used Pd-based membranes, the measured data from the fluidised bed membrane reactor could be well described, provided that axial gas back-mixing in the membrane-assisted fluidised bed reactor is negligible. This indicates that the membrane reactor behaviour approached that of an ideal isothermal plug flow reactor with maximum H_2 permeation.

Keywords: Hydrogen production; Fluidised beds; Membrane reactors; Small scale power production

1. Introduction

The suitability of polymer electrolyte membrane fuel cells (PEMFC) for stationary and vehicular applications, because of its low operating temperatures, compactness, higher power density, cleaner exhausts and higher efficiencies compared to conventional internal combustion engines and gas turbines, adds to the already soaring demand for hydrogen production for refinery and petrochemical applications (Carrette et al., 2001; Lattner and Harold, 2004). A complete transition from commercially mature fossil fuel-based routes to hydrogen as a future energy carrier based on sustainable processes with newly emerging renewable fuel resources will require at least a few decades to be realised. In this interim period, efficient and careful use of fossil-based resources is required, which demands for alternative technologies that can minimise anthropogenic emissions and optimise the process performance. For small scale applications (typically up to 200 kW), perm-selective H_2

* Corresponding author. Tel.: +31 534894478; fax: +31 534892882.
E-mail address: m.vansintannaland@tnw.utwente.nl
(M. van Sint Annaland).

0009-2509/$ - see front matter © 2007 Elsevier Ltd. All rights reserved.
doi:10.1016/j.ces.2007.02.022

membrane-based processes (combining H_2 separation and hydrocarbon fuel processing in a single unit operation) are considered more attractive compared to the commercially mature routes such as steam reforming and autothermal reforming of methane (SRM/ATR) because of the inherent smaller reactor volume and reduced number of process units via process integration and intensification. H_2 is conventionally produced from CH_4 using a combination of steam reformers coupled with water–gas-shift (WGS) units and a downstream train of separators to minimise CO and CH_4 in the product (Rostrup-Nielsen, 1984, 2002). The SRM/WGS reactions are limited by their thermodynamic equilibriums, but can be shifted in favourable direction by selectively removing H_2 via a perm-selective membrane, so that maximum CH_4 conversion and CO shift can be accomplished, thereby maximising the H_2 product yield, while simultaneously H_2 is obtained in ultrapure form (< 10 ppm CO) directly usable in downstream PEMFCs (Adris et al., 1994; Kikuchi, 1995, 2000; Aasberg-Petersen et al., 1998). The endothermic heat requirement of SRM can be met, as is done industrially in the case of ATR, by partially combusting or oxidising CH_4 using air or pure oxygen (Bharadwaj and Schmidt, 1995; Pena et al., 1996; Aasberg-Petersen et al., 2001; Wilhelm et al., 2001). When using air, CO_2 separation from the reaction product (which will be mainly N_2 because of minimal CH_4 and CO slip) is cost intensive and difficult, requiring additional separation units. Use of pure O_2 necessitates cryogenic air distillation, which becomes uneconomical at smaller scales of operation. The use of perm-selective O_2 membranes for distributive O_2 feeding can solve the problems associated with the energy requirementof the process and CO_2 capture simultaneously (Balachandran et al., 1995, 1997; Dixon, 1999, 2003; Hendriksen et al., 2000; Maiya et al., 2000).

Different reactor types have been considered for the proposed application and their feasibility for integrated operation and optimum reactor performance has been assessed (Patil, 2005). Because of the ease of operation and availability of a commercial catalyst for ATR, packed bed membrane reactors (PBMRs) are the obvious first choice. To evaluate the feasibility of performing ATR in a PBMR with perm-selective H_2 membranes, a two-dimensional pseudo-homogeneous PBMR model has been developed. This model describes the axial and radial temperature and concentration profiles in the catalyst bed, by solving the component mass and energy balances coupled with the total continuity and Navier–Stokes equations to account for the effect of the H_2 extraction on the flow profiles. Simulations have shown that indeed autothermal operation can be achieved by co-feeding the O_2. However, large temperature excursions have been predicted at the reactor inlet, which are detrimental for membrane life and catalyst performance. Different operation modes, such as cooling the reactor wall with sweep gas or staged feeding of O_2 have been evaluated and only minor improvements in moderating the temperature peaks can be achieved at the expense of a much more complicated and cost-intensive reactor design and reduced H_2 product yield and CO shift. Concentration polarisation (i.e., mass transfer limitations from the catalyst bed to the membrane surface) because of the selective H_2 removal has been found to manifest itself with increasing membrane permeability thereby constraining the reactor design. To decrease the adverse effects of mass transfer limitations to the membrane wall, a small membrane tube diameter needs to be selected. It has been shown that because of the relatively small ratio of the membrane tube diameter to the particle diameter, the porosity profile in the catalyst bed needs to be taken into account in order to prevent overestimation of the H_2 removal rate. It was concluded that, in principle autothermal production of H_2 in a PBMR is feasible, provided that the membranes are positioned outside the inlet region, where large temperature gradients prevail (Kurten, 2003; Kurten et al., 2004; Tiemersma et al., 2006).

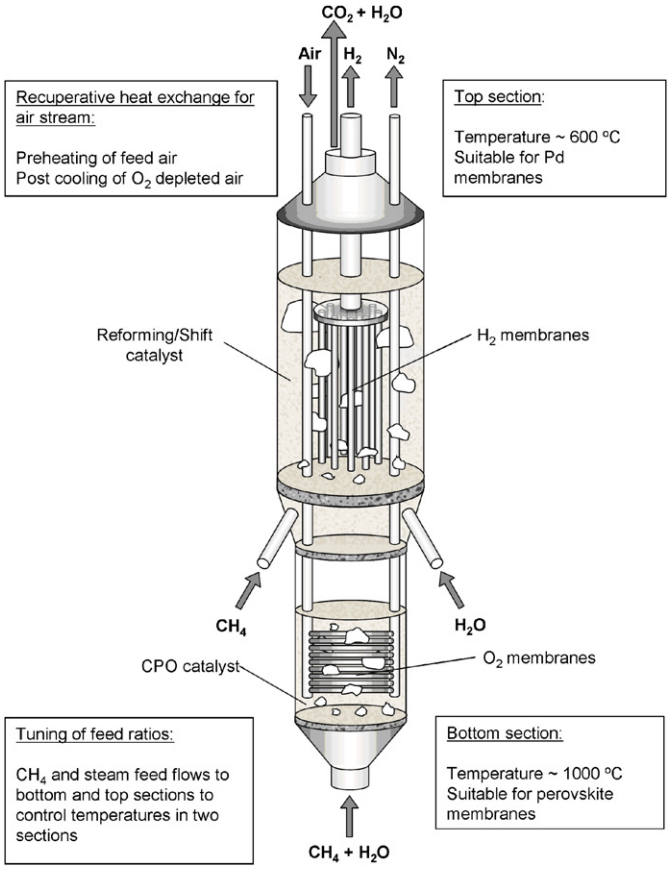

Fig. 1. Schematic of the novel reactor concept (Kuipers et al., 2006).

In view of the operational constraints concurrent with the relatively large axial and radial temperature and concentration gradients and difficulties in inserting both H_2 and O_2 membranes in a PBMR, it is proposed to integrate all the unit operations in a novel fluidised bed membrane reactor owing to its excellent heat transfer characteristics and ease of inserting membranes. The proposed novel membrane-assisted fluidised bed reactor consists of a partial oxidation bottom section and a SRM/WGS top section (see Fig. 1). Because of the large difference in operating temperatures of the perm-selective H_2 membranes (below 700 °C) and perm-selective O_2 membranes (above 900 °C), two sections operate at these respective temperatures. The fraction of CH_4 feed is fed through the bottom section in such a way that the permeating O_2 is able to generate

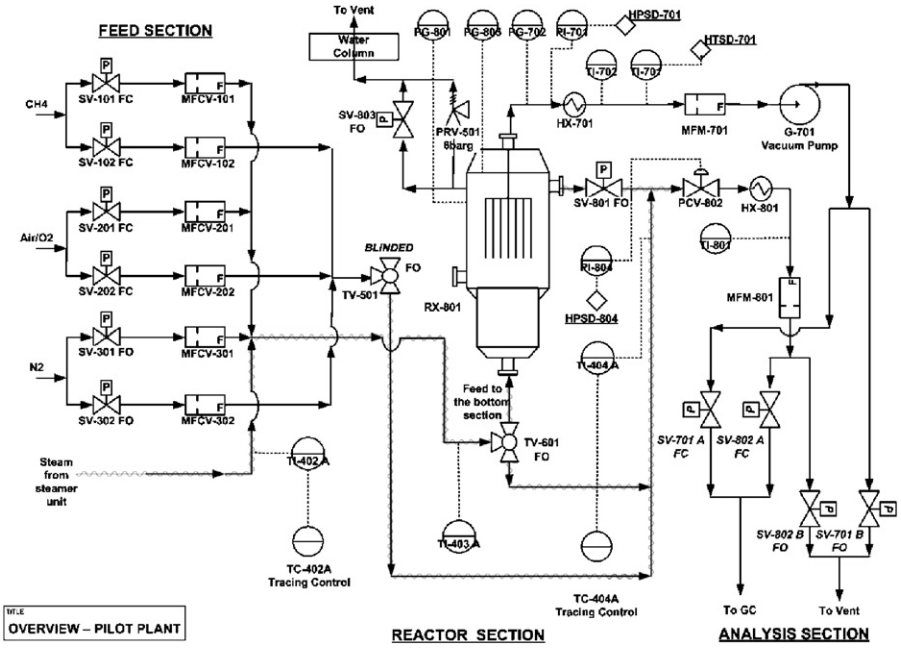

Fig. 2. Process flow diagram of the pilot plant setup.

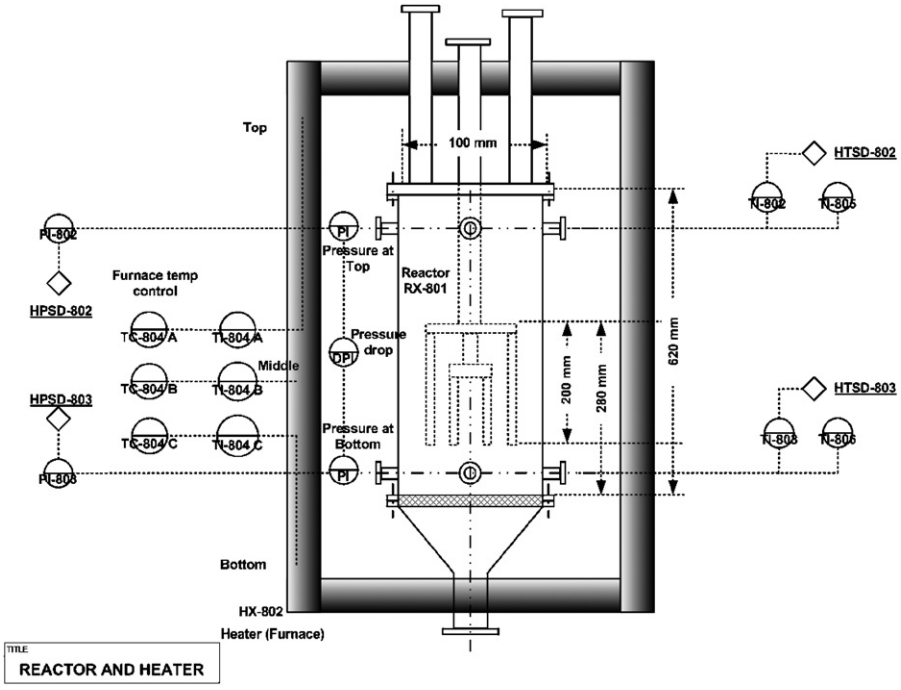

Fig. 3. Details of the reactor and heater section with safety shutdowns and heating controls (HPSD—high pressure shut down, HTSD—high temperature shut down).

CPO (catalytic partial oxidation) equilibrium conditions in the bottom section, temperatures of which are in turn favourable for the perm-selective O_2 transport. The steam is also added to avoid coke formation in the bottom section. The top section is then fed with the remaining CH_4 and steam feed so that overall autothermicity is achieved when viewed over both the sections. The endothermic heat demand of the top section is thus catered by the equilibrium mixture coming from the bottom section and the side feed of additional CH_4 and steam. In the bottom section O_2 is introduced selectively via dense perovskite membranes in order to supply the required reaction energy via CPO for the steam reforming/WGS reactions in the top section, where H_2 is selectively extracted via dense Pd-based membranes thereby surpassing the thermodynamic

Fig. 4. Picture of the (a) fluidised bed membrane reactor and (b) membrane assembly.

equilibrium limitations. Using thermodynamic equilibrium calculations and more detailed fluidised bed membrane reactor modelling, it has been demonstrated that autothermal operation and effective temperature control in both reaction sections can be achieved along with high CH_4 conversions and H_2 yields by tuning the overall CH_4 and steam feed ratios and the feed ratios to the bottom and top sections (Patil, 2005; Patil et al., 2005, 2006; Kuipers et al., 2006).

The development of tubular perovskite membranes with high oxygen permeation fluxes and high stability and durable sealing of these ceramic membranes into a reactor is still a subject of extensive research world-wide. Hence, it has been decided to undertake a stepwise demonstration of the concept, starting with an experimental proof of principle for the top section of the reactor. A reliable sealing of the Pd-based membranes in the top section had already been developed by the manufacturer (Buxbaum and Hsu, 1992; Buxbaum and Kinney, 1996; Buxbaum, 2002, 2004). Very good stability of the membrane and the sealing has been experimentally demonstrated. On the basis of a separately developed expression for the H_2 permeation rate through the membranes and information on the steam reforming reaction rates on a commercial noble metal-based catalyst (Patil, 2005), a fluidised bed membrane reactor for the non-autothermal steam reforming of CH_4 was designed and constructed.

Table 1
Alumina and catalystyst particles data and correlations used for calculating minimum fluidisation velocity (u_{mf})

	Particle size (μm)	Particle density ($kg\,m^{-3}$)	Geldart classification
Alumina	104	1670	B
Catalyst	300–500	3400	B

Correlations used for calculating u_{mf}.
Archimedes number (Kunni and Levenspiel, 1991)

$$Ar = \frac{d_p^3 \rho_g (\rho_p - \rho_g) g}{\mu_g^2}.$$

Minimum fluidisation velocity (Shiau and Lin, 1993)

$$u_{mf} = \left(\frac{\mu_g}{\rho_g d_p}\right)\left(\sqrt{(27.2)^2 + 0.0408 Ar} - 27.2\right).$$

First a single membrane prototype of the unit was built and tested (Patil et al., 2006). Based on the operational experience with this unit, a 10 Pd membranes unit was designed for H_2 production via SRM for a power output with PEMFC in the range of 50–100 W. In the next section, the pilot scale demonstration unit is described in detail showing the process flow diagram. Subsequently, experiments to determine the minimum

fluidisation velocity of the bed inventory (consisting of a mixture of a commercial noble metal-based catalyst and inert alumina particles) are described. Experimental results for the SRM at different superficial gas velocities (1.5–6u_{mf}), different temperatures (550–650 °C) and pressures (2–4 bar) are presented. Some experiments have been repeated with the addition of an extra amount of catalyst to investigate the influence of reaction kinetics. The results in terms of CH_4 conversion, CO selectivity, H_2 product yield and H_2 flux or power output are compared with thermodynamic equilibrium predictions accounting for the H_2 permeation. Then, a more general phenomenological model is developed to describe the membrane-assisted fluidised bed reactor, accounting for bubble-to-emulsion phase mass transfer, reaction kinetics and axial gas back-mixing in the emulsion phase. Finally, the paper concludes with a summary of the most important outcomes and an outlook for future research on this topic.

2. Fluidised bed membrane reactor for SRM

2.1. Description of the setup

A fluidised bed membrane reactor for the SRM was designed and constructed (see Fig. 1). The setup is fully automated and a user interface was developed in Labview. The setup consists of three sections; a feed section, a reactor section and an analysis section.

Feed section: The feed section (see Fig. 2) consists of the feed gases supply from gas cylinders (CH_4, CO, CO_2, N_2 and H_2 from Indugas b.v. and Hoekloos b.v.) and mass flow controllers (MFCs) to set the desired flow rates and gas composition (Smart Mass Flow type from Brooks b.v.). All gas supply lines are additionally protected with pneumatically operated shut off valves (Nypro type) to cut-off gas supply in case of an emergency shutdown. A steam generation unit for (small) laboratory scale operation involves a HPLC pump (Biotronic BT-8100 series) to feed a precise amount of water into an electrical furnace that generates steam and the pressure is controlled using a series of check valves. The steam supply lines and the reactor exhaust lines are insulated and covered with electrical heat tracing to maintain the temperature sufficiently high to avoid water condensation and pressure fluctuations in the reactor due to droplet formation.

Reactor section: The reactor section consists of the fluidised bed membrane reactor of 10 cm diameter and 60 cm height (see Fig. 3). It is heated using three electric furnaces (baby ovens) of 2.2 kW capacity each. The pressures at bottom and top of the reactor, on the downstream of the reactor and on the permeate side upstream of the vacuum pump are measured using pressure transmitters (PTX 1400 from Druck b.v.). K-type thermocouples (from Rossel b.v.) are used to measure the temperature in the reactor (at the top and bottom) and for the control of the electric heaters (top, middle and bottom). The feed to the reactor can be bypassed using a 3-way valve (Parker type) so that its composition can be analysed. Additionally, the reactor is equipped with safety features. There are two high temperature and three high pressure shutdowns to avoid runaways and damage to the membrane tubes, the reactor and downstream equipment. There is an additional high pressure and temperature shutdown on the permeate side to protect the mass flow meter and avoid explosive mixtures in the vacuum pump in the event of a membrane rupture or seal failure. Moreover, the setup is equipped with explosive gas and CO detectors. In case a hazardous and/or poisonous gas mixture is detected outside the reactor an emergency shutdown is triggered. Ten dead-end Pd-based membranes have been inserted (procured from REB Research, Ferndale, US; dimensions 3.2 mm diameter and 20 cm length) inside the reactor, connected via a tree structure to the

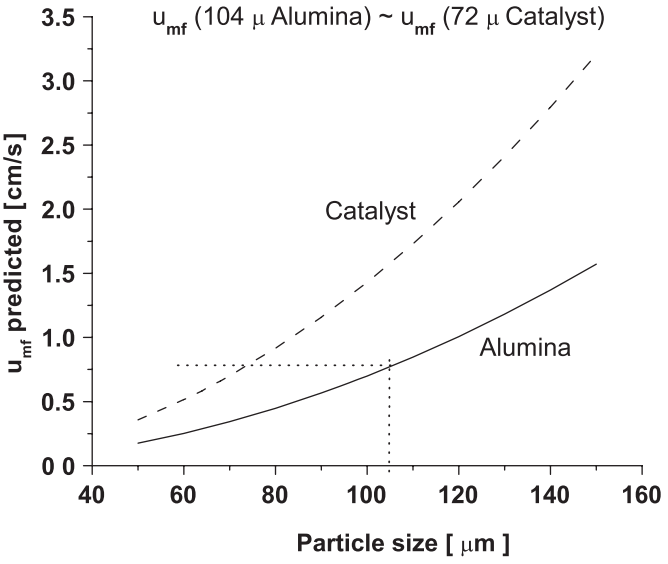

Fig. 5. Predictions of u_{mf} for alumina and catalyst particles as a function of the particle size.

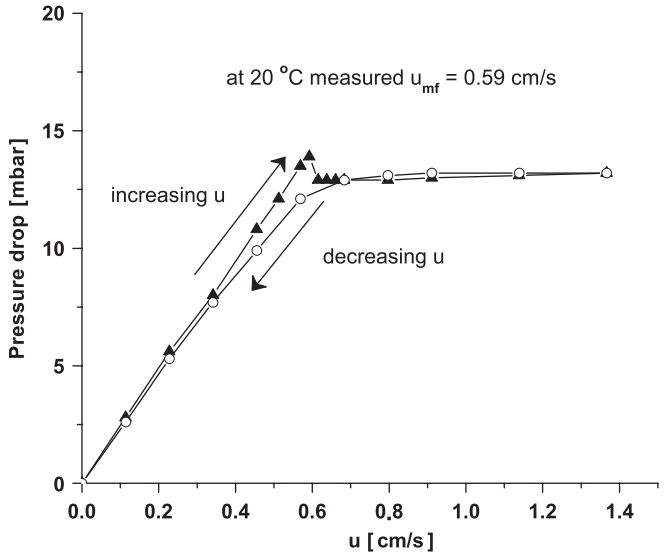

Fig. 6. Experimental determination of u_{mf} using pressure drop measurements at room temperature.

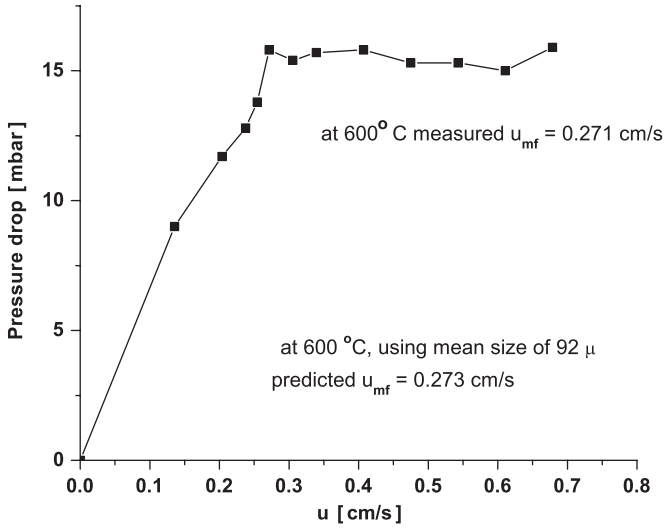

Fig. 7. Experimental measurements of u_{mf} at 600 °C.

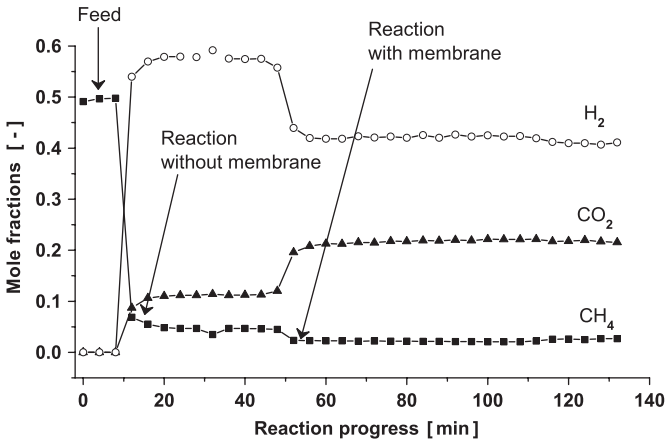

Fig. 8. Typical feed and product composition as a function of time during an experiment.

permeate side of the reactor. The membranes consist of a metal tube reinforced with Inconel with a dense 4–5 μm Pd layer deposited on both sides. The reactor tube and membrane tree assembly are depicted in Fig. 4. The catalyst used for the steam reforming experiments was supplied by Shell Global Solutions International b.v. and is a highly active noble metal-based CPO catalyst. Concluded from kinetics experiments (Patil, 2005), only a very small amount of this catalyst is required for the design H_2 production capacity, which necessitates the use of diluent particles such as inert alumina for creating sufficient bed height for complete immersion of the Pd membranes in the suspension. By conducting experiments in the pilot plant without catalyst and inert particles, it was ensured that the contribution of gas phase reactions is negligible. Moreover, the reactor metal tube (stainless steel) and the alumina particles also exhibited no catalytic activity within the investigated operating temperatures and pressures.

Table 2
Overview of operating conditions and measurements

Catalyst amount (g)	50
Catalyst size (μm)	50–75
Alumina amount (g)	1400
Alumina size (μm)	104
Catalyst/alumina (wt%)	3.5
Bed height at u_{mf} (cm)	28
L/D ratio at u_{mf}	2.8
Feed ratio mol N_2/mol CH_4	1
Feed ratio mol H_2O/mol CH_4	4
Pressure range (bar)	2, 3 and 4
Temperature range (°C)	550, 600 and 650
u/u_{mf} range	1.5, 2, 3, 4 and 6

The alumina particles procured from Aldrich (activated neutral Brockmann type of 150 mesh size) had a high surface area (155 $m^2\,g^{-1}$) and hence it was sintered for 24 h at 900 °C to convert the γ-phase into the α-phase and reduce the surface area and acidity.

Analysis section: The analysis section comprises of a μ-GC (CP-4900 series from Varian b.v.) equipped with two Mol-sieve (5 Å) columns and a Poraplot Q (PPQ) column to analyse the gas streams. One of the mol-sieve columns is used for detecting CH_4, CO, N_2 and O_2 while the other is used to detect H_2 or He. The PPQ is used to measure CO_2 concentration and traces of water. It is possible to sample both the reactor exhaust (retentate) and product H_2 (permeate) streams.

2.2. Experimental measurement of the minimum fluidisation velocity

The minimum fluidisation velocity (u_{mf}) is one of the most important parameters in fluidised bed operation, as it signifies the onset of fluidisation and determines the fluidisation regime (such as bubbling or turbulent fluidisation). Based on the measurements of the bulk densities of the alumina and catalyst particles as listed in Table 1, u_{mf} was calculated for both the alumina and catalyst particles as a function of the particle size (see Fig. 5). For a catalyst particle size of ~72 μm approximately the same u_{mf} is predicted as for the 104 μm alumina particles so that particle segregation can be avoided. To experimentally verify this, a mixture of 50–75 μm catalyst and 104 μm alumina particles was fluidised in a small glass test bed and was indeed found to fluidise homogeneously and mix uniformly. Subsequently, this mixture with a large dilution of alumina particles because of the high activity of the catalyst (50 g catalyst +1.4 kg alumina) was placed in the fluidised bed reactor such that the membrane assembly was completely submerged in the gas–solid suspension under minimum fluidisation conditions (see Fig. 3).

Subsequently, the minimum fluidisation velocity of the catalyst/alumina particle mixture was determined experimentally by measuring the pressure difference over the bed at different fluidisation velocities. As expected, the measured pressure drop differs slightly when measured for increasing velocity in a packed bed and decreasing velocity in a fluidised bed due

Table 3
Comparison of measured data with equilibrium data for (a) without membranes and (b) with membranes, for different fluidisation velocities at 550 °C and 2 bar

u/u_{mf} at 2 bar abs pressure	Measured data			Equilibrium data
	1.5	2	3	
(a)				
Methane conversion (%)	58.47	57.04	56.00	59.93
H_2/CO ratio	18.09	18.58	18.87	21.73
CO selectivity	0.20	0.20	0.20	0.18
H_2/CH_4 reacted	3.78	3.76	3.76	3.82
Error in C balance (%)	−1.79	−1.42	−0.64	
Approach to equilibrium (%)	97.56	95.18	93.45	

u/u_{mf} at 2 bar abs pressure	Measured data			Equilibrium data		
	1.5	2	3	1.5	2	3
(b)						
Methane conversion (%)	87.62	80.64	70.47	93.61	88.73	79.73
H_2/CO ratio	7.41	9.09	12.30	9.66	11.01	13.55
CO selectivity	0.10	0.12	0.13	0.10	0.12	0.14
H_2/CH_4 reacted	3.90	3.88	3.87	3.89	3.87	3.85
Power (W)	53.04	59.73	61.37			
Separation factor (SF)	0.80	0.73	0.57			
Error in C balance (%)	−2.18	0.92	−1.18			
Approach to equilibrium (%)	93.60	90.89	88.39			

to the well-known hysteresis effect. Based on these measurements with nitrogen at room temperature, u_{mf} was found to be 0.59 cm s^{-1}, which corresponds to a mean particle size of 92 μm using the correlations from Table 1 (see Fig. 6). The reactor was then heated to 600 °C and the pressure drop measurements were repeated. The experimental results indicated a u_{mf} of 0.271 cm s^{-1}, which matched reasonably well with the predictions based on the correlation listed in Table 1 using a mean particle size of 92 μm and a particle density of the alumina particles (see Fig. 7).

2.3. Standard operating procedure

A standard operating procedure was developed and followed for all the measurements to maintain consistency and comparability in the experimental data. First the temperature in the reactor was stabilised at the desired value using the heaters. The steam pump was started and the steam generator was stabilised in a closed loop, i.e., without adding steam to the reactor section. Then, the desired feed flow rates (CH_4 and N_2) were set in the reactor bypass mode to measure the feed composition on the μ-GC. Subsequently, steam was added in the bypass mode and the pressure was stabilised. During all these steps, overall mass balance was verified using the reactor exhaust mass flow meter (MFM 801, see Fig. 2). Thereafter, the feed was introduced into the reactor and the change in pressure and temperature was monitored. The pressure rises due to the net mole production and hence the outlet flow increases relative to the feed flow. The reactor was first operated in a non-membrane mode in which the permeate side was blocked to prevent flow of H_2 through the membrane. The reactor outlet was sampled continuously and the dry product composition was determined to calculate the conversion and selectivities. N_2 was used as a reference inert gas to check the carbon mass balance (which was always within ±5% error). Once the product composition was determined, the membrane side was unblocked and H_2 permeated using a vacuum pump (G 701) to maximise the driving force for the H_2 flux. Again, the product composition was measured with the μ-GC and the change in the reactor performance because of the selective H_2 extraction was compared with the case without membrane permeation. The measured product composition in time during a typical experiment is shown in Fig. 8. This figure shows that when the feed flow of CH_4 and steam, first stabilised in the reactor bypass mode, is fed to the fluidizing catalyst, the reactions start immediately. First the operation is stabilised while the permeate side of the membranes are blocked, and subsequently membrane permeation is activated, which can be seen in the marked decrease in the CH_4 concentration at the outlet and the increased CO_2 concentration due to the enhanced shift reaction.

3. Experimental results

The parameters that were used to quantify the reactor performance are defined as follows:

$$\text{Methane conversion} = \frac{\phi_{CH_4,in} - \phi_{CH_4,out}}{\phi_{CH_4,in}}$$

$$H_2/CO \text{ ratio} = \frac{\phi_{H_2,unpermeated}}{\phi_{CO,out}}$$

$$\text{CO selectivity} = \frac{\phi_{CO,out}}{\phi_{CO,out} + \phi_{CO_2,out}}$$

$$H_2/CH_4 \text{ reacted} = \frac{\phi_{H_2,total}}{\phi_{CH_4,reacted}}$$

Power output (W)	$=H_2$ flux (mol/s) $\times 10^{5}$[a]
Separation factor (SF)	$=\dfrac{\phi_{H_2,\text{permeated}}}{\phi_{H_2,\text{total}}}$
Approach to equilibrium	$=\dfrac{\text{Methane conversion}_{\text{measured}}}{\text{Methane conversion}_{\text{equilibrium}}}$

[a]The power output was calculated using the lower heating value of 242 kJ mol^{-1} for H_2 and a fuel cell efficiency of 40% (Brown, 2001).

The nitrogen mole balance was used to calculate the reactor exhaust concentrations from the dry sample stream composition analysed with the μ-GC in order to account for the increase or decrease in the total molar flow rate because of the chemical reactions and H_2 extraction. The carbon balance is defined as follows:

$$C_{\text{balance}} = \text{mol}_{CH_4,\text{in}} - \text{mol}_{CH_4,\text{out}} - \text{mol}_{CO,\text{out}} - \text{mol}_{CO_2,\text{out}}.$$

The following sets of experiments were carried out (summarised in Table 2).

- Variation of the fluidisation velocity at a fixed pressure of 2 bar.
- Variation of the pressure for a fixed throughput.
- Variation of the temperature for the above two sets.

In the next sections, the experimental results are tabulated, plotted and discussed. When referring to measurements without the membranes, it should be understood that in these measurements the before-described reactor unit was used with the membrane bundle physically present inside, however, where H_2 was not extracted. First, experimental results with and without the membranes are compared with thermodynamic equilibrium calculations accounting for the H_2 extraction. The extent of the enhancement in the reactor performance because of the perm-selective H_2 extraction is investigated for different fluidisation velocities, pressures and temperatures.

3.1. Effect of fluidisation velocity and pressure

3.1.1. Effect of fluidisation velocity at 550 °C and 2 bar

Experiments were carried out at 550 °C and 2 bar pressure for different fluidisation velocities (u/u_{mf}) of 1.5, 2 and 3 (see Table 3 and Figs. 9 a–c). The CH_4 conversion for the case without the membranes approached the equilibrium predictions closely indicating that sufficient catalyst was used to overcome most of the kinetic limitations. However, the approach to equilibrium decreased with increasing throughput pointing towards the existence of kinetic and/or mass-transfer limitations at higher velocities at this temperature. As will be shown later, at higher temperatures the approach to equilibrium is slightly increased, indicating a small effect of kinetic limitations at this temperature. The important advantage of the membrane reactor, i.e., the possibility to surpass the thermodynamic equilibrium because of H_2 extraction, reflected in increased CH_4 conversion, increased ratio of mole H_2 produced/CH_4 reacted and decreased CO selectivity, is clearly shown in Fig. 9. As the throughput is increased, this enhancement decreases indicating that the H_2 permeation through the membranes becomes the limiting factor determining the reactor performance at higher fluidisation velocities. This is also reflected in a minor

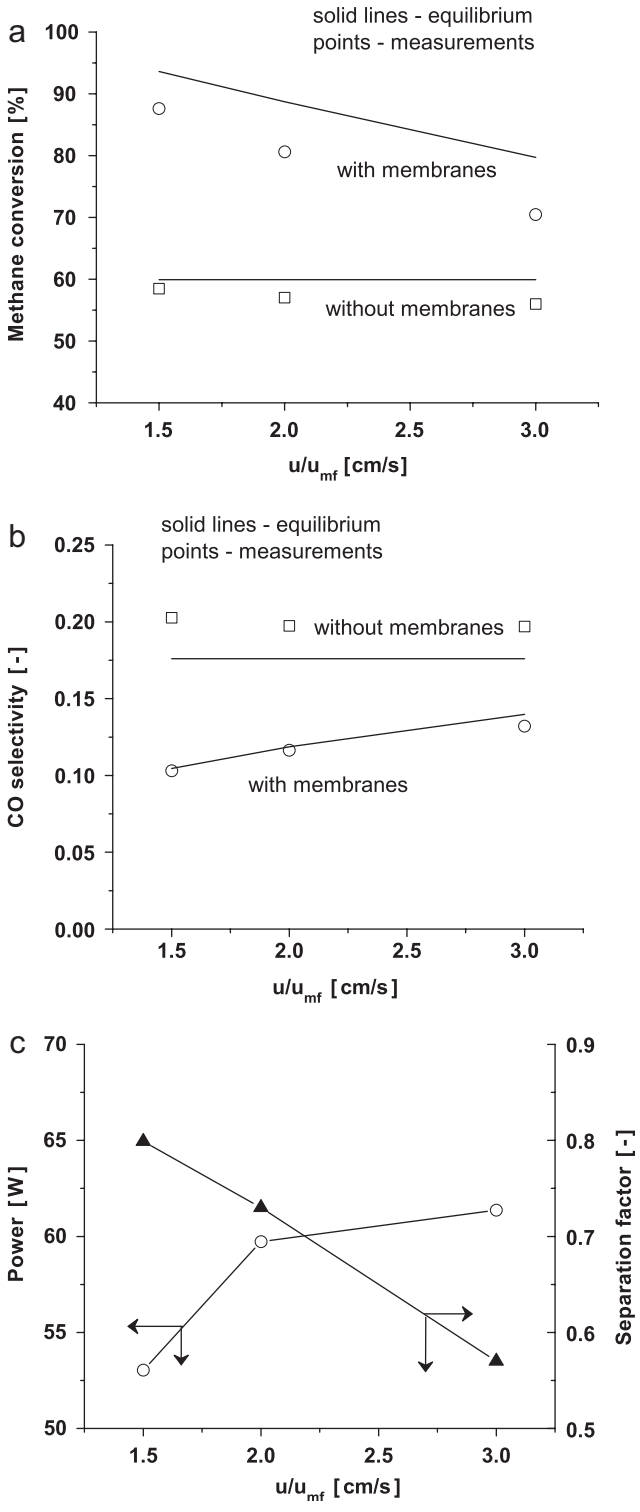

Fig. 9. (a) Methane conversion, (b) CO selectivity and (c) power output and H_2 separation factor, for different fluidisation velocities at 550 °C and 2 bar.

Table 4
Comparison of measured data with equilibrium data for (a) without membranes and (b) with membranes, at different pressures for the same throughput at 550 °C

Pressure (bar abs) [$3u_{mf}$ at 2 bar]	Measured data			Equilibrium data		
	2	3	4	2	3	4
(a)						
Methane conversion (%)	56.00	49.41	45.09	59.93	52.55	47.68
H_2/CO ratio	18.87	21.59	22.08	21.73	25.14	27.98
CO selectivity	0.20	0.17	0.17	0.18	0.15	0.14
H_2/CH_4 reacted	3.76	3.82	3.81	3.82	3.85	3.86
Error in Cbalance (%)	−0.64	−1.46	−1.70			
Approach to equilibrium (%)	93.45	94.03	94.58			
(b)						
Methane conversion (%)	70.47	68.83	68.95	79.73	78.37	77.82
H_2/CO ratio	12.30	10.73	11.31	13.55	13.44	13.31
CO selectivity	0.13	0.11	0.09	0.14	0.12	0.10
H_2/CH_4 reacted	3.87	3.89	3.91	3.85	3.87	3.90
Power (W)	61.37	71.34	77.88			
Separation factor (SF)	0.57	0.68	0.74			
Error in C balance (%)	−1.18	−0.76	−0.09			
Approach to equilibrium (%)	88.39	87.82	88.60			

improvement in the power output for the case with the membranes for u/u_{mf} of 2 and 3 (from 59.7–61.4 W). This suggests the use of higher temperatures to increase the membrane permeability or higher reactor pressures to increase the driving force for H_2 permeation. The power output increases with increasing throughput at the expense of higher H_2 losses via the reactor exhaust (i.e., lower separation factor) and lower CH_4 conversions (see Fig. 9c). In all these cases, it can be seen that the WGS is favoured towards completion, as the CO selectivity drops from 20% for the case without membranes down to 10% for the case with membranes.

3.1.2. Effect of pressure at 550 °C at constant throughput

The operating pressure was increased from 2 to 4 bar keeping the feed throughput same, meaning lower u/u_{mf} at higher pressures. The operating pressure affects the thermodynamic equilibrium and the membrane permeation flux (see Table 4 and Figs. 10 a–c). The CH_4 conversion for the case without membranes decreases with increasing pressure because of the unfavourable shift in the SRM equilibrium (Fig. 10a). On the other hand, for the case with the membranes the CH_4 conversion remains almost the same indicating that the unfavourable shift in the equilibrium is compensated for by an increase in the H_2 permeation. Thus, the CH_4 conversion is increased by 125% at 2 bar pressure, 140% at 3 bar and 152% at 4 bar, showing higher benefits of perm-selective H_2 extraction at higher pressures. The power output is also increased from 61 to 78 W for the same feed throughput by doubling the reactor pressure, while the separation factor is increased from 57% to 74% indicating less H_2 slip via the reactor exhaust. The CO selectivity depends on the extent of the WGS reaction which is independent of the pressure, but influenced by CH_4 conversion and H_2 extraction. A higher H_2 flux shifts the WGS equilibrium and the CO selectivity is lowered from 13% to 9%.

These results indicate that operation at higher pressure is favoured because of the higher fluxes (increased power output and separation factor) and lower CO selectivities. Moreover, from the results it can be concluded that the reactor performance is determined by the H_2 permeation fluxes. The maximum CH_4 conversion (87.4%) achieved at $1.5u_{mf}$ at 2 bar is still below desired values (< 95%). At higher temperatures, the membrane permeability is improved resulting in higher H_2 permeation fluxes and thus improved reactor operation, as will be shown next.

3.1.3. Experiments at 600 and 650 °C for different fluidisation velocities and operating pressures

When operated at 600 °C and 2 bar for different fluidisation velocities (ranging from 2 to $6\,u_{mf}$) the CH_4 conversion without membranes is close to equilibrium values, while with the membranes, the conversion is improved significantly because of the increased H_2 permeation at higher temperatures (see Figs. 11 a–c). Because the fluidisation velocity is increased over a wide range, the membrane flux became limiting at higher throughputs and the advantages gained because of the higher temperature were counterbalanced by large CH_4 and H_2 losses in the reactor exhaust (81% CH_4 conversion and 38% separation factor at $6u_{mf}$). As the pressure is varied for the same throughput at 600 °C, similar trends were observed as discussed before in the case of 550 °C (see Figs. 12a–c). Operation at higher pressure (4 bar) improves the power output (111 W) and separation factor (55%), but the feed throughput is too high for the membranes to handle, resulting in higher CH_4 and H_2 losses.

Results for experiments at 650 °C at fluidisation velocities of 1.5, 2 and 3 times u_{mf} at 2 bar are described in Fig. 13. Using the membranes, it is possible to reach a CH_4 conversion as high as 99.7% for $1.8u_{mf}$ at 2 bar with a CO selectivity of

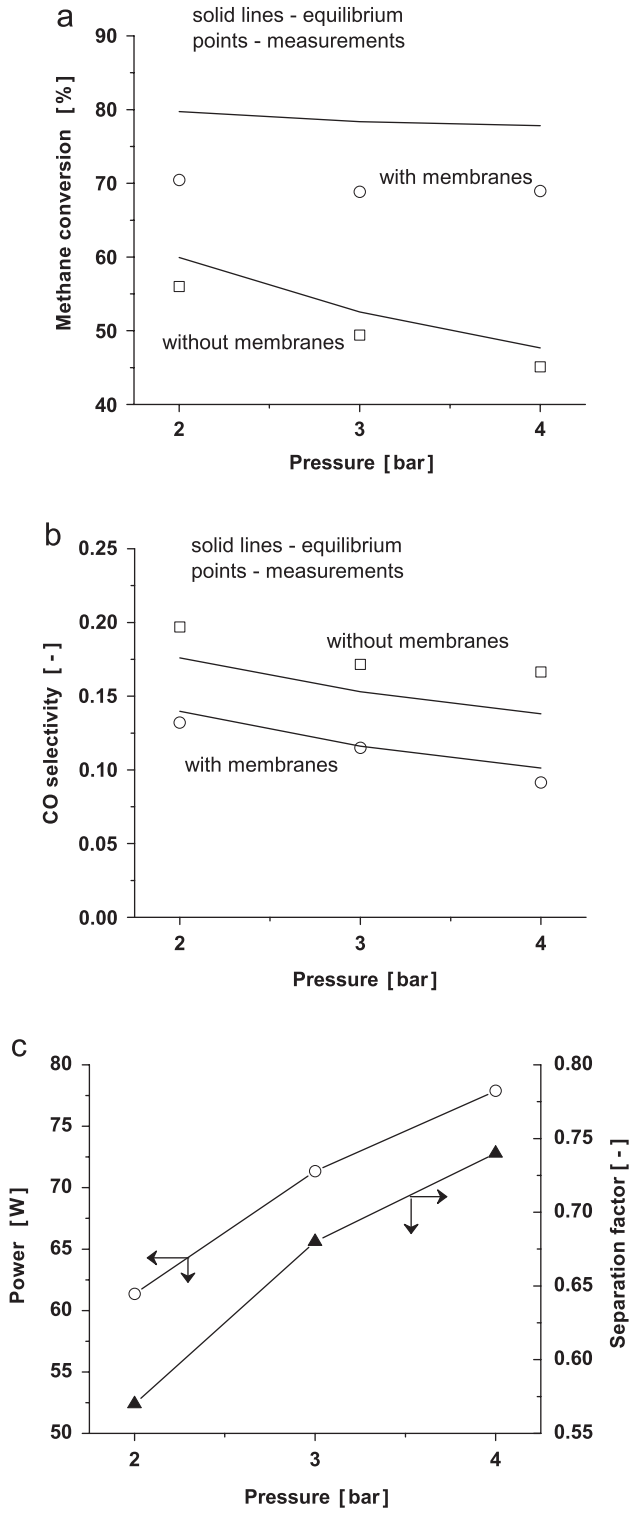

Fig. 10. (a) Methane conversion, (b) CO selectivity and (c) power output and H_2 separation factor, at different pressures for the same throughput at 550 °C.

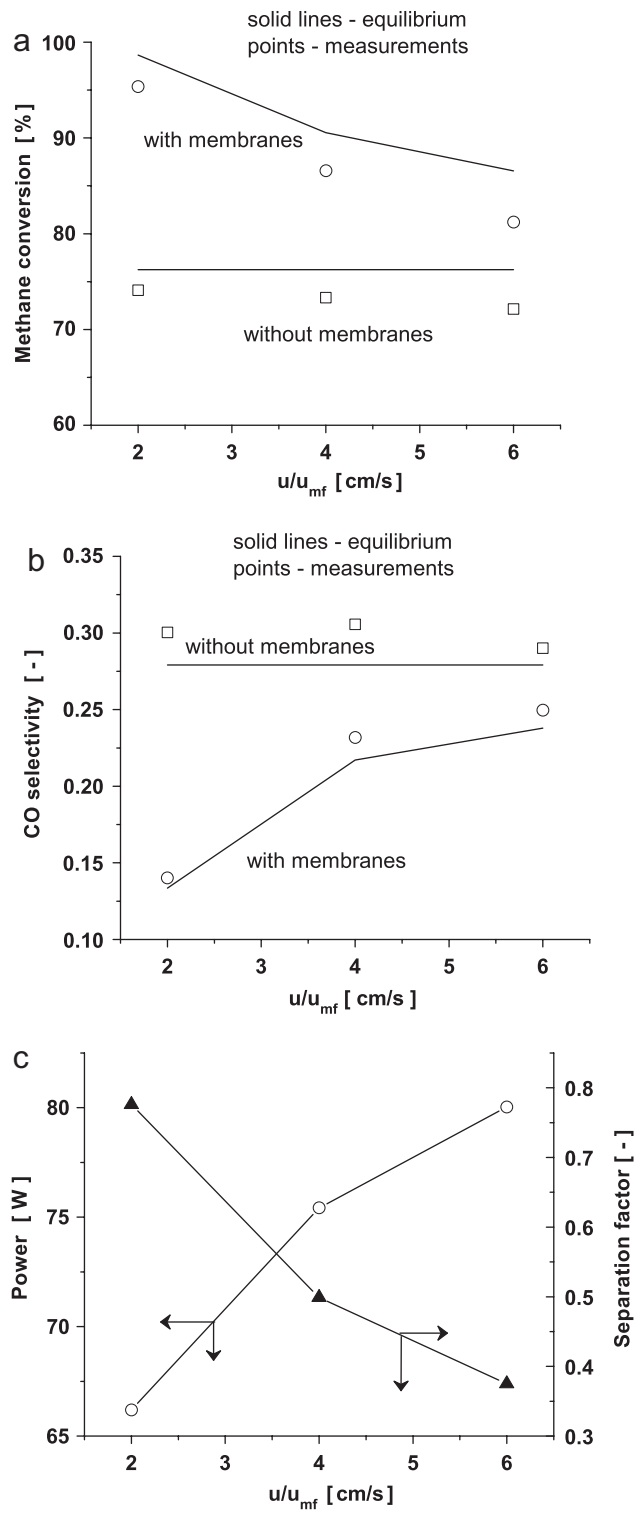

Fig. 11. (a) Methane conversion, (b) CO selectivity and (c) power output and H_2 separation factor, for different fluidisation velocities at 600 °C and 2 bar.

13% and a power output of 61 W with a separation factor of 84% (see Figs. 13a–c). The approach to equilibrium is higher than in previous cases, indicating absence of (particularly) kinetic and mass transfer limitations at higher temperatures and relatively low fluidisation velocities. On the other hand, it is more difficult to shift WGS towards completion at higher temperatures because of unfavourable shift in the equilibrium and a large fraction of H_2 (separation factors > 80%) needs to be permeated to achieve CO selectivities below 15%. Increasing the pressure from 2 to 4 bar for the same feed throughput

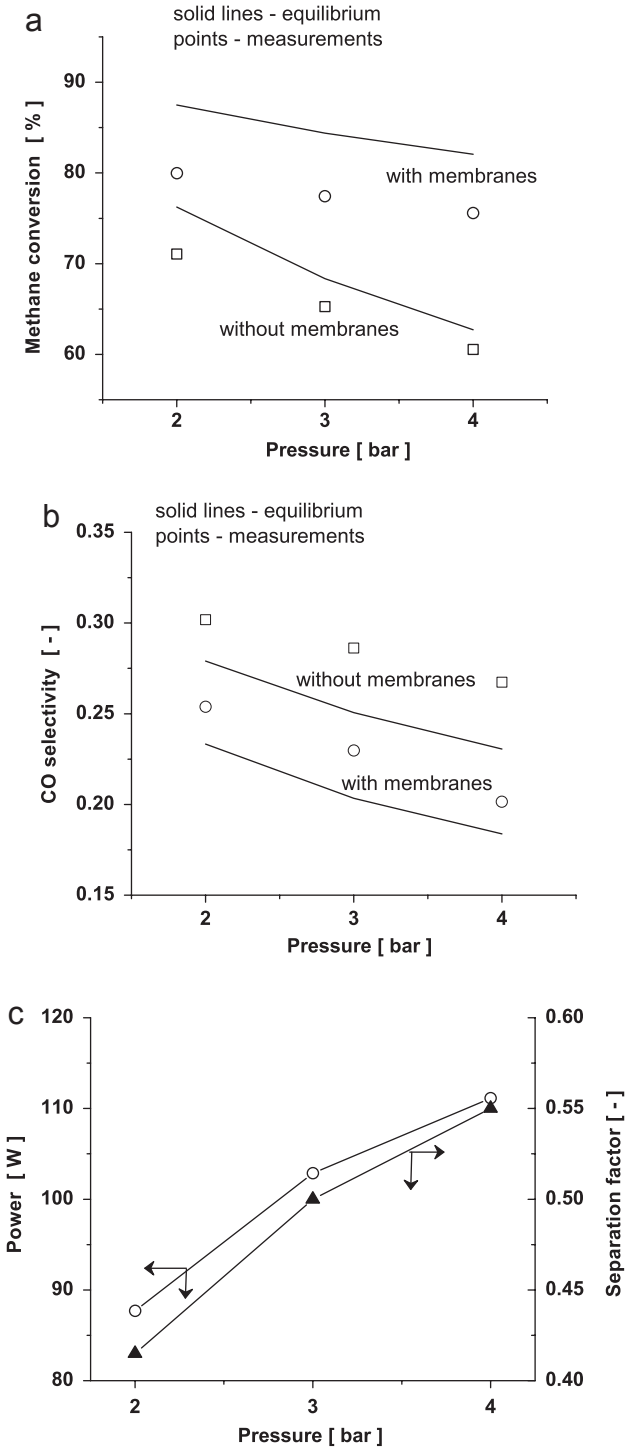

Fig. 12. (a) Methane conversion, (b) CO selectivity and (c) power output and H_2 separation factor, at different pressures for the same throughput at 600 °C.

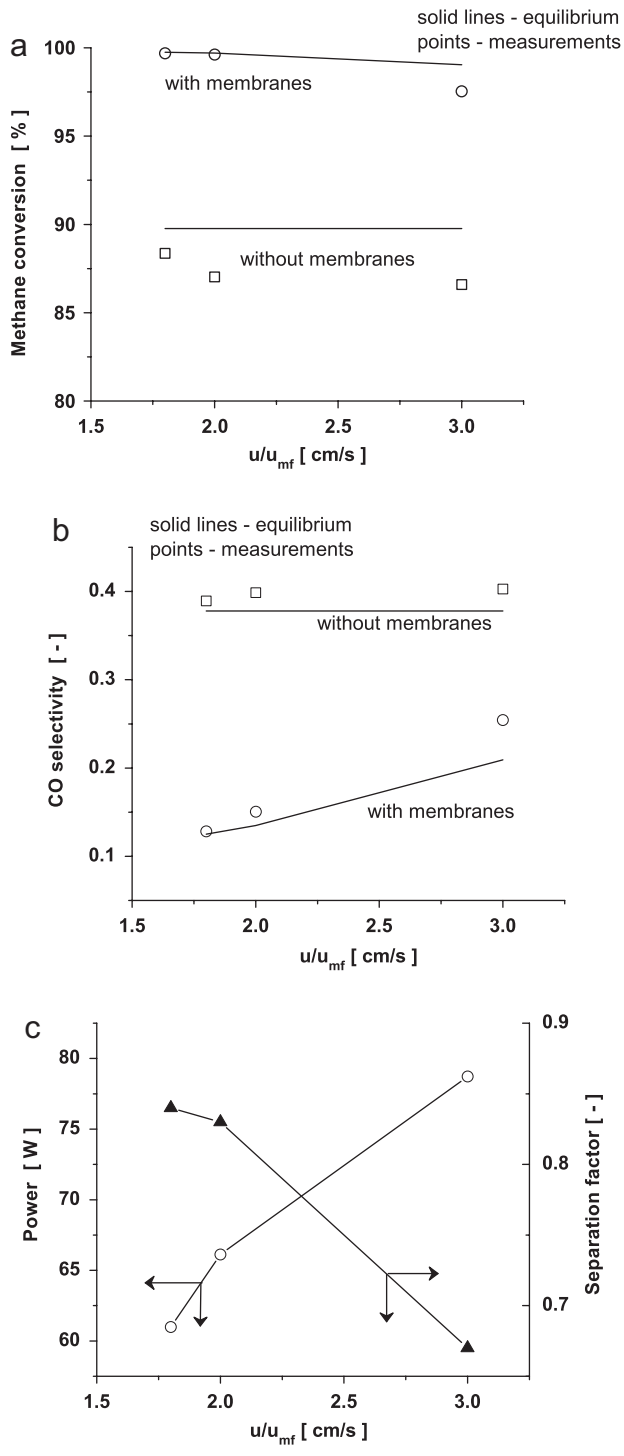

Fig. 13. (a) Methane conversion, (b) CO selectivity and (c) power output and H_2 separation factor, for different fluidisation velocities at 650 °C and 2 bar.

(see Figs. 14 a–c) resulted in an increased power output (from 78 to 102 W) and a higher separation factor (from 67% to 87%), while the CH_4 conversion dropped marginally (from 97.5% to 97.2%) indicating that operation at higher pressures and temperatures is preferred.

3.2. Effect of temperature

The effect of temperature is shown for the same fluidisation velocity at two different pressures to get a better insight into the reactor performance. Comparison of the experimental results at 2 bar (see Figs. 15a–c) indicates that operation at

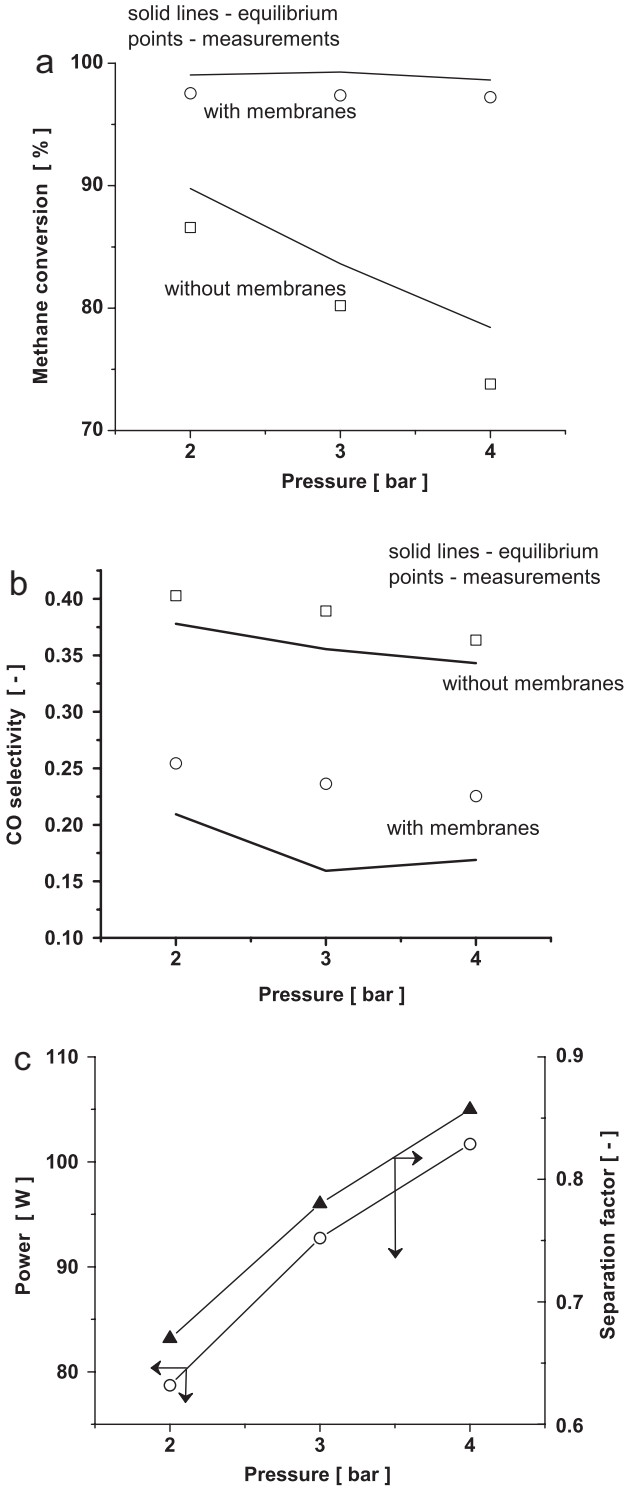

Fig. 14. (a) Methane conversion, (b) CO selectivity and (c) power output and H_2 separation factor, at different pressures for the same throughput at 650 °C.

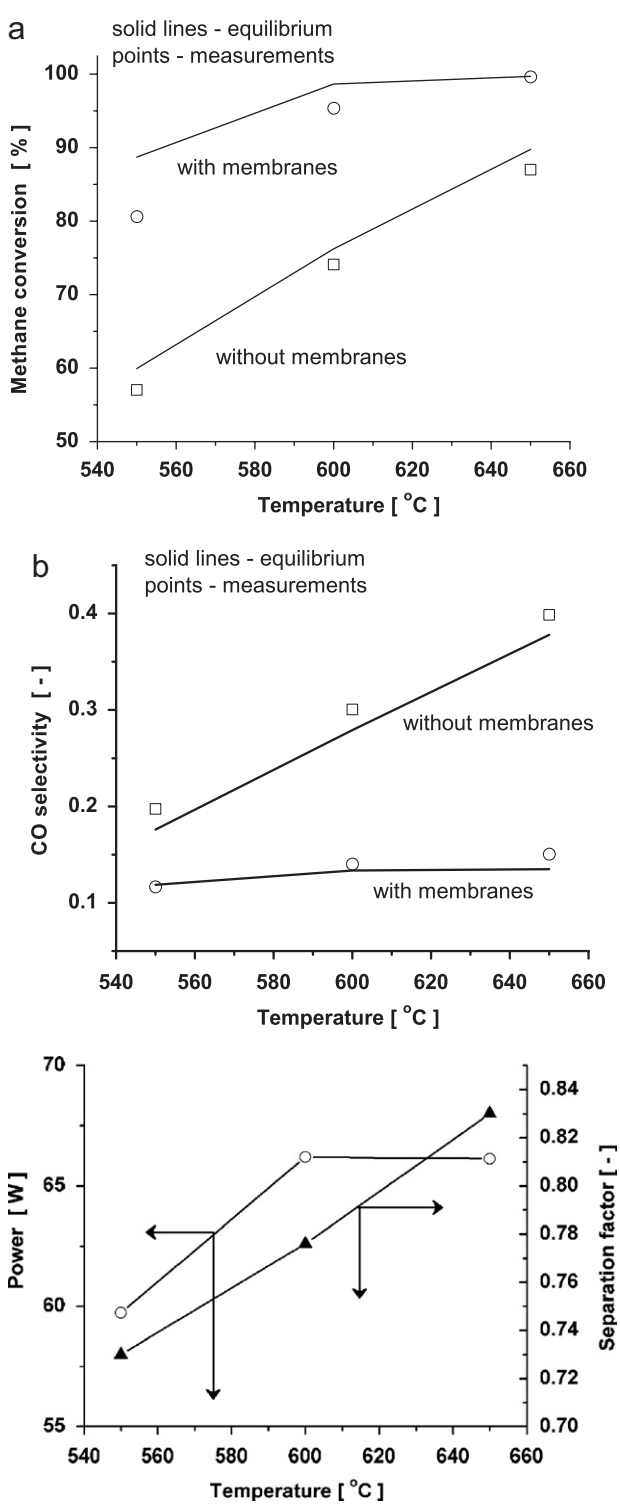

Fig. 15. Effect of temperature on (a) methane conversion, (b) CO selectivity and (c) power and separation factor, for a fixed pressure of 2 bar at $2u_{mf}$.

a temperature of 650 °C gives the best performance in terms of CH_4 conversion (99.6% at 650 °C compared to 80.6% at 550 °C) because of the increased permeation. Without membranes, the measured conversions are close to the equilibrium values for all the temperatures (96% approach to equilibrium), while for the cases with membranes the approach to equilibrium improves with higher temperatures (at 650 °C 99.9% approach to equilibrium) because of the increased reaction rates. The power output increases slightly from 60 W at 550 °C to 66 W at 650 °C, however, the separation factor at 650 °C is 83%

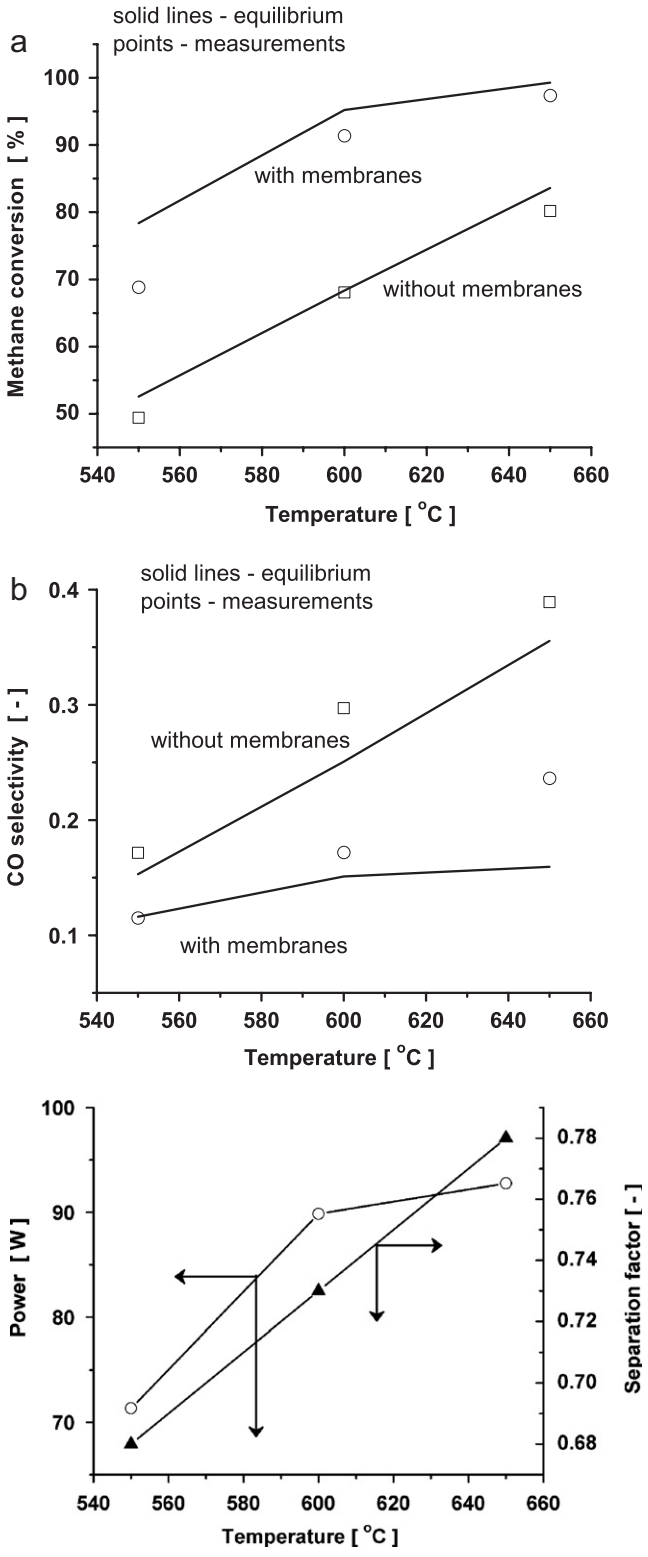

Fig. 16. Effect of temperature on (a) methane conversion, (b) CO selectivity and (c) power and separation factor, for a fixed pressure of 3 bar at $2u_{mf}$.

compared to 73% at 550 °C, indicating a lower H_2 slip via the reactor exhaust because of the higher permeability at higher temperatures.

The experimental results at 3 bar (see Figs. 16a–c) indicate that at higher pressures, the power output is increased (at 650 °C from 66 W at 2 bar to 93 W at 3 bar), but the separation factor is decreased (from 83% at 2 bar to 78% at 3 bar) due to the higher throughput (1.5 times) at 3 bar compared to 2 bar. The CH_4 conversion drops from 99.6% (2 bar) to 97.4% (3 bar), but the improvement over the case without membranes is 121% (3 bar) compared to 114% (2 bar). From these results the optimal operating window can be identified.

Operating conditions		Reactor performance	
Temperature (°C)	650	CH_4 conversion	> 97%
Pressure (bar)	3–4	CO selectivity	< 15%
Throughput (u/u_{mf})	1.5–2	H_2/CH_4 reacted	> 3.7
		Power output (W)	75–100
		Separation factor	0.8–0.9

3.3. Kinetic and mass transfer limitations

To elucidate the contribution of kinetic reaction rate limitations on the reactor performance, experiments at 550 °C were repeated with the addition of extra 25 g of catalyst to the original catalyst/alumina mixture. As can be seen from Table 5, the approach to equilibrium improves only by 1% for the cases without membranes, indicating that there are hardly any kinetic limitations and that the small differences between the measured and the equilibrium conversions are mainly caused by (small) mass transfer limitations. Interestingly, for the case with the membranes, the approach towards the equilibrium is more enhanced (almost by 5%) with the added amount of catalyst. This can be explained by the strongly increased conversion, requiring the additional catalyst to reform the additional amount of CH_4 compared to the case without membranes. As seen from previous sections, the approach to equilibrium at 600 and 650 °C with 50 g catalyst is even higher than at 550 °C and therefore these experiments were not repeated at higher temperatures. One experiment at 600 °C using 75 g of catalyst matched very well with the data for 50 g catalyst confirming the absence of kinetic limitations at higher temperatures.

4. Model validation

4.1. Equilibrium model

As can be concluded from the results presented in the previous section, the fluidised bed membrane reactor operates close to the thermodynamic equilibrium conditions (approach to equilibrium above 98%), particularly at 650 °C, where only the permeation of H_2 through the membranes is accounted for. Thus, with a thermodynamic equilibrium model combined with a lumped flux expression for H_2 permeation (Patil, 2005), it is possible to reasonably well predict the reactor performance beforehand. The equilibrium reactor model essentially assumes very fast reaction kinetics and bubble-to-emulsion

Table 5
Comparison of CH_4 conversion for additional amount of catalyst

u/u_{mf} at 2 bar pressure	Measured data		Equilibrium		Approach	
	2	3	2	3	2	3
(a) Without membranes						
50 g *catalyst*						
Methane conversion (%)	57.04	56.00	59.93	59.93	95.18	93.45
75 g *catalyst*						
Methane conversion (%)	57.68	56.64	59.93	59.93	96.25	94.52
(b) With membranes						
50 g *catalyst*						
Methane conversion (%)	80.64	70.47	88.73	79.73	90.89	88.39
75 g *catalyst*						
Methane conversion (%)	85.04	75.44	89.33	81.70	95.20	92.35

Table 6
Comparison of the equilibrium model predictions with the measured data at 600 °C and 2 bar at $2u_{mf}$ and $CH_4: H_2O: N_2 = 1:4:1$

Base case at 600 °C $2u_{mf}$ at 2 bar abs pressure	Measured data	Equilibrium model predictions
Methane conversion (%)	95.37	96.84
CO selectivity	0.14	0.17
H_2 flux (Nml min^{-1})	890	778
Separation factor (SF)	0.78	0.68

phase mass transfer and completely back-mixed emulsion and bubble phases. However, when using this equilibrium model discrepancies in the H_2 flux or separation factor and CO selectivity are found (see Table 6). Hence, a more detailed reactor model has been developed to assess the origin of the discrepancies between the equilibrium model and the experimental data.

4.2. Membrane-assisted fluidised bed reactor model (*MAFBR*)

The MAFBR model is essentially an extension of the bubble assemblage model, frequently used to describe the phenomena in a fluidised bed reactor (Kato and Wen, 1969), to account for the presence of and the permeation through the membranes. A detailed description of the model assumptions and model equations can be found in the work of Deshmukh and co-workers (Deshmukh, 2004; Deshmukh et al., 2005a,b). By means of modelling and experimental validation, they have shown that the axial gas phase back-mixing in the emulsion phase is strongly reduced by the presence of the membranes and that the addition of gas through the membranes further improves the plug flow behaviour. In this model, the degree of axial back-mixing is represented in terms of the number of continuous ideally stirred tank reactors (CISTRs) in series (N_e for the number of tanks for the emulsion phase and N_b for the number of tanks for the bubble phase relative to that for the emulsion phase), where $N_e = 1$ represents a completely back-mixed emulsion phase (see Fig. 17). Moreover, this model accounts for a net change in the volumetric flow rates because of the chemical reactions and the extraction of the gas via the

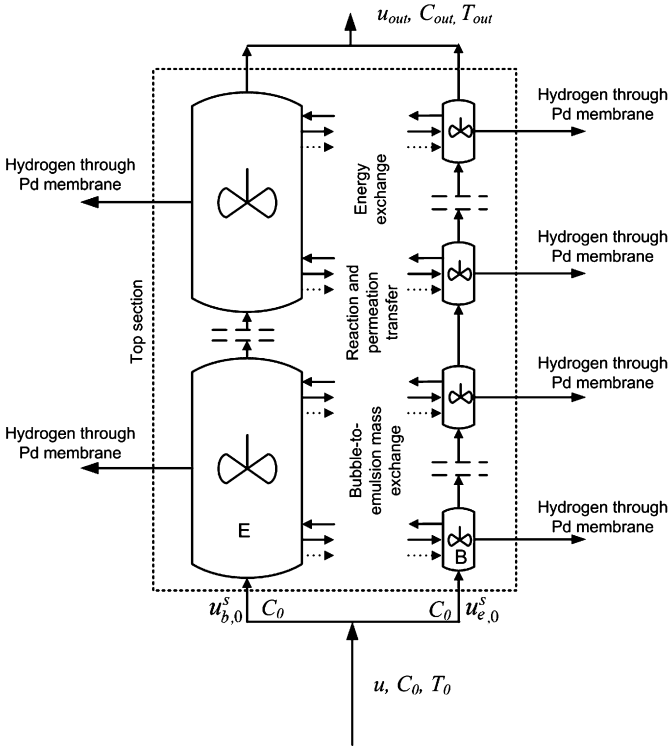

Fig. 17. Schematic for the fluidised bed reactor model.

membranes. The lumped flux expression for H_2 extraction and the reaction kinetics expression for SRM have been incorporated in this model to predict the membrane flux and reactor performance. The closure equations for the hydrodynamic parameters can be found in the work of Deshmukh. The mass balance equations have been summarised in Table 7, the flux equation and the data in Table 8 and the reaction kinetics data in Table 9.

4.3. Reactor performance at 600 °C

4.3.1. Mass transfer limitations

It has been experimentally demonstrated that reaction kinetics are not rate determining because a sufficiently large amount of active catalyst was used. However, the approach to

Table 7
Mass balance equations

Total mass balance

$$u^s_{b,n-1}A_T\rho_{b,n-1} - u^s_{b,n}A_T\rho_{b,n} + u^s_{e,n-1}A_T\rho_{e,n-1} - u^s_{e,n}A_T\rho_{e,n} + \sum_{i=1}^{n_c}\phi^{\text{membrane}}_{i,\text{mol},n}M_{w,i}A_{\text{membrane},n} = 0,$$

where

$$u^s_{e,b}A_T = u_{e,n}A_T(1-e_{b,n}); \quad u^s_{b,0}A_T = u_{\text{tot}}A_T e_{b,0}; \quad u^s_{e,0}A_T = u_{\text{tot}}A_T(1-e_{b,0})$$

Transfer term

$$Q = u^s_{e,n-1}A_T\rho_{e,n-1} - u^s_{e,n}A_T\rho_{e,n} + \sum_{i=1}^{n_c}\phi^{\text{membrane}}_{i,\text{mol}}A_{\text{membrane}}(1-e_{b,n}) + \sum_{i=1}^{n_c}K_{be,i,n}V_{b,n}\rho_{b,n}(\omega_{b,i,n}-\omega_{e,i,n})$$

Bubble phase component mass balances (for $i = 1, \ldots, n_c$)

$$u^s_{b,n-1}A_T\rho_{b,n-1}\omega_{b,i,n-1} - u^s_{b,n}A_T\rho_{b,n}\omega_{b,i,n} - K_{be,i,n}V_{b,n}\rho_{b,n}(\omega_{b,i,n}-\omega_{e,i,n}) + \phi^{\text{membrane}}_{i,\text{mol}}M_{w,i}A_{\text{membrane}}e_{b,n} + Q[\omega_{e,i,n}H(Q) - \omega_{b,i,n}H(-Q)] = 0$$

Emulsion phase component mass balances (for $i = 1, \ldots, n_c$)

$$u^s_{e,n-1}A_T\rho_{e,n-1}\omega_{e,i,n-1} - u^s_{e,n}A_T\rho_{e,n}\omega_{e,i,n} - K_{be,i,n}V_{b,n}\rho_{b,n}(\omega_{b,i,n}-\omega_{e,i,n}) + \phi^{\text{membrane}}_{i,\text{mol}}M_{w,i}A_{\text{membrane}}(1-e_{b,n})$$
$$+\left(\sum_{j=1}^{n_{\text{rxns}}}\nu_{i,j}r_j\right)(1-\varepsilon_e)\rho_p V_{e,n}M_{w,i} - Q[\omega_{e,i,n}H(Q) - \omega_{b,i,n}H(-Q)] = 0$$

Table 8
Membrane flux data (Patil, 2005)

Flux through Pd based membrane

$$j_{H_2} = \frac{P_{\text{Pd}}}{t_{\text{Pd}}}\cdot\left(p^x_{H_2,\text{feed}} - p^x_{H_2,\text{permeate}}\right)$$

for pressure exponent: $x = a_1\cdot T^2 + a_2\cdot T + a_3$

a_1	a_2	a_3
-3.90979×10^{-6}	4.96376×10^{-3}	-0.569705

for permeability: $\ln P_{\text{Pd}} = b_1\cdot T^2 + b_2\cdot T + b_3$

b_1	b_2	b_3
5.18253×10^{-5}	-6.47388×10^{-2}	-7.23505

Table 9
Reaction rate data (Patil, 2005)

Reaction rate for steam reforming reaction

$$r_{\text{SRM}} = \frac{k_1 p_{CH_4}}{1 + K^{\text{ads}}_{CH_4}p_{CH_4} + K^{\text{ads}}_{CO}p_{CO} + K^{\text{ads}}_{CO_2}p_{CO_2} + K^{\text{ads}}_{H_2}p_{H_2}}$$

Parameter	at 550 °C	at 600 °C	at 650 °C
k_1 (mmol kgcat^{-1} s^{-1} bar^{-1})	1205.8	1407	2435.2
$K^{\text{ads}}_{CH_4}$ (bar^{-1})	4.36	4.36	4.36
K^{ads}_{CO} (bar^{-1})	23.44	9.01	2.91
$K^{\text{ads}}_{CO_2}$ (bar^{-1})	3.74	2.45	1.06
$K^{\text{ads}}_{H_2}$ (bar^{-1})	5.69	6.07	3.17

equilibrium decreases with increasing u/u_{mf} as can be discerned from the measured data (see Table 10), which can be explained by increased bubble-to-emulsion phase mass transfer limitations. To validate this, simulations have been performed with the MAFBR model and compared with the experimental results for the cases without membranes. The experimental data at 600 °C has been selected because of the wider variation in u/u_{mf} investigated, ranging from 2 to 6 compared to 1.5 to 3 at other temperatures (see Table 10).

Assuming at first a completely back-mixed emulsion phase ($N_e = 1$), an increase in the fluidisation velocity indeed results in a decreased conversion as observed experimentally, which can be attributed to a decrease in the bubble-to-emulsion phase mass transfer rate caused by an increase in the average bubble size (see Table 10 and Fig. 18). The number of CISTRs in series assumed for the bubble phase strongly affects the methane conversion. This is not caused by the decreased degree of axial back-mixing in the bubble phase, but is related to the better representation of the change in bubble size along the bed height (see Fig. 18). For high N_b the presence of small bubbles at the bottom of the bed is accounted for enhancing the mass transfer, resulting in increased methane conversion. However, even when assuming an infinite number of CISTRs in the bubble phase (i.e., plug flow in the bubble phase and optimal representation of the bubble growth profile) the experimentally determined methane conversion can still not be reached. The remaining discrepancy is related to the degree of back mixing in the emulsion phase as explained in the next sub-section.

Table 10
Degree of back-mixing in the bubble phase for the case without membranes

u/u_{mf} at 2 bar abs pressure	Measured data			Equilibrium data		
	2	4	6			
Methane conversion (%)	74.10	73.33	72.14	76.25		
Approach to equilibrium (%)	97.18	96.17	94.61			
Model predictions	Methane conversion (%)			Average bubble size (mm)		
u/u_{mf} at 2 bar abs pressure	2	4	6	2	4	6
$N_e = 1$; $N_b = 1$	71.92	66.70	62.60	9.81	14.64	17.96
$N_e = 1$; $N_b = 3$	73.65	71.10	68.64	9.85	14.73	18.28
$N_e = 1$; $N_b = 5$	73.69	71.38	69.22	9.85	14.73	18.10

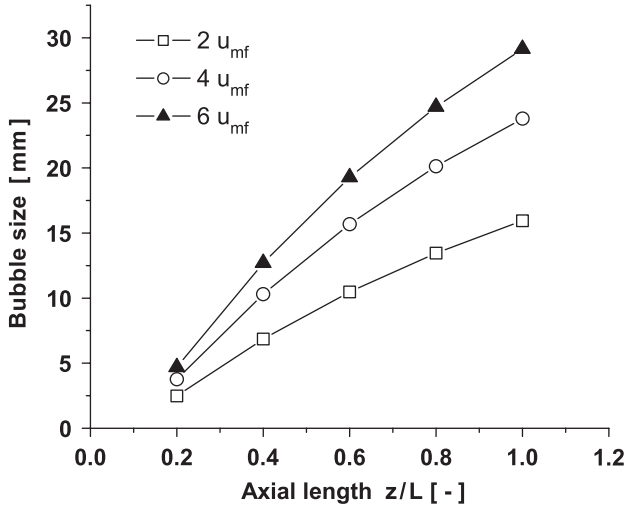

Fig. 18. Bubble growth along the bed height for different fluidisation velocities at 600 °C and 2 bar ($N_e = 1$, $N_b = 5$).

4.3.2. Degree of axial back-mixing in emulsion phase

For the base case (600 °C at 2 bar at $2u_{mf}$ and CH_4:H_2O:N_2= 1:4:1), the effect of the degree of back-mixing in the emulsion phase has been investigated for the case with permeation through the membranes (see Table 11). The degree of axial back-mixing in the bubble phase again influences the CH_4 conversion (comparing $N_b = 1$ and 5 cases), however, the permeated flux through the membranes is not significantly altered by the number of CISTRs in the bubble phase because of the small bubble fraction in the fluidised bed at these relatively low fluidisation velocities, so that almost the entire membrane surface area is submerged in the emulsion phase. Fixing the ratio of the number of bubble phase CISTRs to the number of emulsion phase CISTRs ($N_b = 5$), the degree of back-mixing in the emulsion phase has been reduced by increasing N_e from 1 to 9, where the actual position of H_2 membranes in the reactor has been accounted for in the model. As can be seen from the results in Table 11, the degree of back-mixing in emulsion phase strongly influences the membrane flux. It can be concluded that for $N_e > 6$, the predicted flux matches well with the measured flux, indicating that the membrane reactor can be best described by assuming both the bubble and emulsion phases in plug flow.

4.3.3. Comparison of experiments with MAFBR and equilibrium models

The reactor performance predicted by the equilibrium model and the MAFBR model has been compared with the measured data for different fluidisation velocities (see Table 12 and Figs. 19 and 20, assuming $N_e = 6$ and $N_b = 5$). The MAFBR model predicts the measured data very well, while the equilibrium model deviates, indicating again the absence of axial gas back-mixing in the reactor and its importance for an accurate prediction of the H_2 permeation flux. Because of the operation at relatively low fluidisation velocities, the presence of the membrane bundle and the extraction of gas via the membranes, the gas phase back-mixing in the emulsion phase is very low and the membrane reactor approaches the behaviour of an isothermal plug flow reactor, simultaneously optimising the performance of the membranes (maximum driving force). The differences between the predictions and measured fluxes at higher fluidisation velocities can be explained by the fact that the influence of internals on the bubble size has not been accounted for. At higher velocities larger bubbles are formed which break because of the interaction with the internals, thereby improving the mass transfer rate and avoiding H_2 bypassing through the bubble phase. Although, the MAFBR accounts for a change in bubble size along the bed height because of the reactions as well as H_2 extraction, it does not account for the increased bubble break-up because of the internals, thereby predicting somewhat lower fluxes at higher fluidisation velocities.

5. Conclusions

A pilot plant setup has been designed and constructed to provide for an experimental proof of principle for the top section of the proposed novel reactor concept for ultrapure H_2 production using non-autothermal SRM reactions. Experiments were conducted at different fluidisation velocities (u/u_{mf} of 1.5 to 6), temperatures (550 to 650 °C) and operating pressures (2 to 4 bar). With these experiments, it has been

Table 11
Comparison of MAFBR model predictions with the measured data at 600 °C and 2 bar at $2u_{mf}$ and $CH_4: H_2O: N_2 = 1:4:1$

Base case at 600 °C $2u_{mf}$ at 2 bar abs pressure				Measured data
Methane conversion (%)				95.37
CO selectivity				0.14
H_2 flux (Nml min^{-1})				890
Separation factor (SF)				0.78
MAFBR model predictions				
Degree of back-mixing in bubble phase ($N_e = 1$; N_b variable)				
CISTRs in bubble phase (N_b)	1	3	5	10
Methane conversion (%)	92.44	94.09	94.11	94.11
CO selectivity	0.19	0.19	0.19	0.19
H_2 flux (Nml min^{-1})	751.1	759.4	759.6	759.6
Separation factor (SF)	0.68	0.68	0.68	0.68
Degree of back-mixing in emulsion phase ($N_b = 5$; N_e variable)				
CISTRs in emulsion phase (N_e)	1	3	6	9
Methane conversion (%)	94.11	96.83	97.45	97.63
CO selectivity	0.19	0.16	0.16	0.15
H_2 flux (Nml min^{-1})	759.6	837.3	875.6	888.3
Separation factor (SF)	0.68	0.72	0.75	0.76

Table 12
Comparison of measured data with MAFBR model predictions at 600 °C and 2 bar for different fluidisation velocities

Base case at 600 °C u/u_{mf} at 2 bar abs pressure	Measured data			MAFBR model ($N_e = 6$; $N_b = 5$)		
	2	4	6	2	4	6
Methane conversion (%)	95.37	86.58	81.22	97.45	88.04	82.5
CO selectivity	0.14	0.23	0.25	0.16	0.25	0.30
H_2 flux (Nml min^{-1})	890	1014	1076	876	1004	1027
Separation factor (SF)	0.78	0.50	0.38	0.75	0.49	0.36

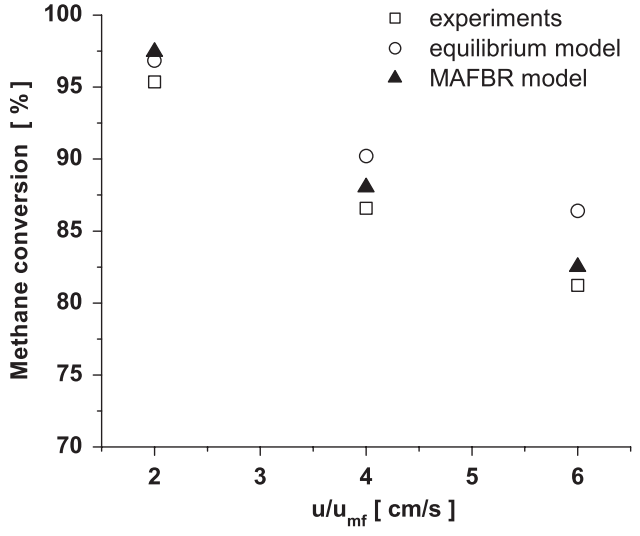

Fig. 19. Comparison of model predictions (equilibrium and MAFBR) with experiments for the methane conversion.

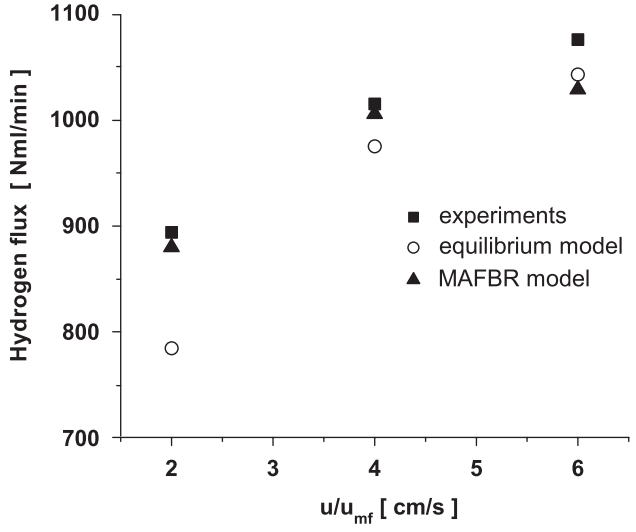

Fig. 20. Comparison of model predictions (equilibrium and MAFBR) with experiments for the H_2 permeation flux.

demonstrated that the reactor performance can be enormously improved with the use of perm-selective H_2 membranes in terms of improved CH_4 conversion, decreased CO selectivity, and improved H_2 product yield and power output. Use of a sufficiently large amount of active noble metal-based catalyst in the experiments has ensured that the operation was carried out in the regime without kinetic rate limitations. Moreover, no problems of coke formation with this catalyst were observed, unlike our experiences with Ni-based commercial SRM catalyst at these temperatures and low steam to CH_4 ratios. Experiments have shown that operation at higher temperatures (650 °C) within the boundaries imposed by membrane stability (i.e., < 700 °C) and higher pressures (which is governed by the limiting membrane flux) gives the best reactor performance. Finally, a phenomenological two-phase model assuming no axial back-mixing in both the bubble and emulsion phases was able to predict the reactor performance forehand with good accuracy showing that the membrane reactor behaviour approached that of the ideal isothermal plug flow reactor, with optimal H_2 permeation.

Notation

$A_{\text{membrane},n}$	membrane surface area per cell n, m^2
Ar	Archimedes number
A_T	area of bed cross-section, m^2
CISTR	continuous ideally stirred tank reactor
d_p	particle diameter, m
g	gravitational constant, $m\,s^{-2}$
$H(Q)$	heaviside function of Q
j_{H_2}	hydrogen flux through the Pd membrane, $mol\,m^{-2}\,s^{-1}$
k_i	reaction rate constant for SRM, $mmol\,kgcat^{-1}\,s^{-1}\,bar^{-1}$
$K_{be,i,n}$	bubble-to-emulsion mass transfer coefficient for component i in cell n, s^{-1}
K_i^{ads}	adsorption constant for component i, bar^{-1}
L/D	length to diameter ratio of catalyst bed in fluidised bed reactor
$\text{mol}_{CH_4,\text{in}}$	molar flow rate of CH_4 fed, $mol\,s^{-1}$
$\text{mol}_{i,\text{out}}$	molar flow rate of component i at outlet, $mol\,s^{-1}$
$M_{w,i}$	molar mass for component i, $kg\,mol^{-1}$
n_c	number of components
n_{rxns}	number of reactions
N_b	number of CISTRs in bubble phase
N_e	number of CISTRs in emulsion phase
$p_{H_2,\text{feed}}$	partial pressure of H_2 on feed side, Pa
$p_{H_2,\text{permeate}}$	partial pressure of H_2 on permeate side, Pa
PID	piping and instrumentation diagram
P_{Pd}	permeability of the Pd membrane, $mol\,m^{-1}\,s^{-1}\,Pa^{-x}$
Q	transfer term accounting for the change in volume
r_j	reaction rate for jth reaction, $mol\,kgcat^{-1}\,s^{-1}$
r_{SRM}	reaction rate for SRM (kinetics studies—Table 9), $mmol\,kgcat^{-1}\,s^{-1}$
SRM	steam reforming of methane
t_{Pd}	thickness of the Pd membrane, m
T	temperature, K
u	superficial velocity at local conditions, $m\,s^{-1}$
$u^s_{L_1,L_2}$	superficial velocity for phase L_1 and cell L_2, $m\,s^{-1}$
u_{mf}	minimum fluidisation velocity, $m\,s^{-1}$
u_{tot}	velocity at bed inlet, $m\,s^{-1}$
V_{L_1,L_2}	volume for phase L_1 and cell L_2, m^3
WGS	water gas shift

Greek letters

ε_e	emulsion phase porosity
μ_g	gas viscosity, Pa s
$v_{i,j}$	stoichiometric coefficient for jth reaction and ith component
ρ_g	gas density, $kg\,m^{-3}$
ρ_p	particle density, $kg\,m^{-3}$
ρ_{L_1,L_2}	density of phase L_1 and cell L_2, $kg\,m^{-3}$
ϕ_i	molar flow of component i, $mol\,s^{-1}$
$\phi^{\text{membrane}}_{i,\text{mol},n}$	molar flux for component i through the membrane per cell, $mol\,m^{-2}\,s^{-1}$
ω_{L_1,L_2,L_3}	weight fraction for phase L_1, component L_2 and cell L_3

Subscripts

0	reactor inlet
b	bubble phase
e	emulsion phase
i	component i
j	number of reactions
n	number of CISTRs for emulsion or bubble phase

Acknowledgements

The authors would like to thank the excellent team of technicians (R. Brouwer, B. Knaken, W. Leppink and R. Meijer) for the construction of the setup and J. Smit for his help in the instrumentation and data acquisition part. Moreover G.J. Kramer (Shell Global Solutions International b.v.) is thanked for availing the noble metal-based catalyst.

References

Aasberg-Petersen, K., Nielsen, C.S., Jorgensen, S.L., 1998. Membrane reforming for hydrogen. Catalysis Today 46 (2–3), 193–201.

Aasberg-Petersen, K., Bak Hansen, J.-H., Christensen, T.S., Dybkjaer, I., Christensen, P.S., Stub Nielsen, C., Winter Madsen, S.E.L., Rostup-Nielsen, J.R., 2001. Technologies for large scale gas conversion. Applied Catalysis A: General 221 (1–2), 379–387.

Adris, A.M., Lim, C.J., Grace, J.R., 1994. The fluidized bed membrane reactor (FBMR) system: a pilot scale experimental study. Chemical Engineering Science 49, 5833–5843.

Balachandran, U., Dusek, J.T., Mieville, R.L., Poeppel, R.B., Kleefisch, M.S., Pei, S., Kobylinski, T.P., Udovich, C.A., Bose, A.C., 1995. Dense ceramic membranes for partial oxidation of methane to syngas. Applied Catalysis A: General 133 (1), 19–29.

Balachandran, U., Dusek, J.T., Maiya, P.S., Ma, B., Mieville, R.L., Kleefisch, M.S., Udovich, C.A., 1997. Ceramic membrane reactor for converting methane to syngas. Catalysis Today 36 (3), 265–272.

Bharadwaj, S.S., Schmidt, L.D., 1995. Catalytic partial oxidation of natural gas to syngas. Fuel Processing Technology 42 (2–3), 109–127.

Brown, L.F., 2001. A comparative study of fuels for on-board hydrogen production for fuel-cell-powered automobiles. International Journal of Hydrogen Energy 26 (4), 381–397.

Buxbaum, R.E., 2002. Hydrogen generator. US Patent 6461408.

Buxbaum, R.E., 2004. Membrane reactors, fundamental and commercial advantages for methanol reforming. ⟨http://www.rebresearch.com/MRessay.html⟩.

Buxbaum, R.E., Hsu, P.C., 1992. Method for plating palladium. US Patent 5149420.

Buxbaum, R.E., Kinney, A.B., 1996. Hydrogen transport through tubular membranes of palladium coated tantalum and niobium. Industrial and Engineering Chemistry Research 35, 530–537.

Carrette, L., Friedrich, K.A., Stimming, U., 2001. Fuel cells—fundamentals and applications. Fuel Cells 1, 5–39.

Deshmukh, S.A.R.K., 2004. Membrane assisted fluidized bed reactor: experimental demonstration for partial oxidation of methanol. Ph.D. Thesis, University of Twente, The Netherlands.

Deshmukh, S.A.R.K., Laverman, J.A., Cents, A.H.G., van Sint Annaland, M., Kuipers, J.A.M., 2005a. Development of a membrane assisted fluidised bed reactor 1. Gas phase back mixing and bubble to emulsion phase mass transfer using tracer injection and ultrasound experiments. Industrial and Engineering Chemistry Research 44, 5955–5965.

Deshmukh, S.A.R.K., Laverman, J.A., van Sint Annaland, M., Kuipers, J.A.M., 2005b. Development of a membrane assisted fluidised bed reactor 2. Demonstration for the partial oxidation of methanol. Industrial and Engineering Chemistry Research 44, 5966–5976.

Dixon, A.G., 1999. Innovations in catalytic inorganic membrane reactors. In: Spivey, J.J. (Ed.), Specialist Periodical Reports: Catalysis. Royal Society of Chemistry, London, 14, 40–92.

Dixon, A.G., 2003. Recent research in catalytic inorganic membrane reactors. International Journal of Chemical Reaction Engineering 1, R6.

Hendriksen, P.V., Larsen, P.H., Mogensen, M., Poulsen, F.W., Wiik, K., 2000. Prospects and problems of dense oxygen permeable membranes. Catalysis Today 56 (1–3), 283–295.

Kato, K., Wen, C., 1969. Bubble assemblage model for fluidized bed catalytic reactors. Chemical Engineering Science 24, 1351–1369.

Kikuchi, E., 1995. Palladium/ceramic membranes for selective hydrogen permeation and their application to membrane reactor. Catalysis Today 25 (3–4), 333–337.

Kikuchi, E., 2000. Membrane reactor application to hydrogen production. Catalysis Today 56 (1–3), 97–101.

Kuipers, J.A.M., Patil, C.S., van Sint Annaland, M., 2006. Process and reactor for the production of hydrogen and carbon dioxide. US Patent Application publication 0013762 A1.

Kunni, D., Levenspiel, O., 1991. Fluidization Engineering. Wiley, New York.

Kurten, U., 2003. Modelling of packed bed membrane reactors: impact of oxygen distribution on conversion and selectivity in partial oxidation systems. Ph.D. Thesis, University of Twente, The Netherlands.

Kurten, U., Sint Annaland, M., Kuipers, J.A.M., 2004. Oxygen distribution in packed bed membrane reactors for partial oxidation systems and its effect on product selectivity. International Journal of Chemical Reaction Engineering 2, A24.

Lattner, J.R., Harold, M.P., 2004. Comparison of conventional and membrane reactor fuel processors for hydrocarbon-based PEM fuel cell systems. International Journal of Hydrogen Energy 29 (4), 393–417.

Maiya, P.S., Anderson, T.J., Mieville, R.L., Dusek, J.T., Picciolo, J.J., Balachandran, U., 2000. Maximizing H_2 production by combined partial oxidation of CH_4 and water gas shift reaction. Applied Catalysis A: General 196 (1), 65–72.

Patil, C.S., 2005. Membrane reactor technology for ultrapure hydrogen production. Ph.D. Thesis, University of Twente, The Netherlands.

Patil, C.S., van Sint Annaland, M., Kuipers, J.A.M., 2005. Design of a novel autothermal membrane assisted fluidized bed reactor for the production of ultrapure hydrogen from methane. Industrial and Engineering Chemistry Research 44, 9502–9512.

Patil, C.S., van Sint Annaland, M., Kuipers, J.A.M., 2006. Experimental study of a membrane assisted fluidised bed membrane reactor for H_2 production by steam reforming of CH_4. Chemical Engineering Research and Design 84, 1–6.

Pena, M.A., Gomez, J.P., Fierro, J.L.G., 1996. New catalytic routes for syngas and hydrogen production. Applied Catalysis A: General 144 (1–2), 7–57.

Rostrup-Nielsen, J.R., 1984. Catalytic steam reforming. In: Anderson, J.R., Boudart, M. (Eds.), Catalysis Science and Technology, vol. 5. Springer, Berlin.

Rostrup-Nielsen, J.R., 2002. Syngas in perspective. Catalysis Today 71 (3–4), 243–247.

Shiau, C.-Y., Lin, C.-J., 1993. An improved bubble assemblage model for fluidized-bed catalytic reactors. Chemical Engineering Science 48 (7), 1299–1308.

Tiemersma, T.P., Patil, C.S., van Sint Annaland, M., Kuipers, J.A.M., 2006. Modelling of packed bed membrane reactors for autothermal production of ultrapure hydrogen. Chemical Engineering Science 61, 1602–1616.

Wilhelm, D.J., Simbeck, D.R., Karp, A.D., Dickenson, R.L., 2001. Syngas production for gas-to-liquids applications: technologies, issues and outlook. Fuel Processing Technology 71 (1–3), 139–148.